POLITECNICO DI TORINO
Repository ISTITUZIONALE

Real Time Energy Management Control Strategies for an Electrically Supercharged Gasoline Hybrid Vehicle

Original
Real Time Energy Management Control Strategies for an Electrically Supercharged Gasoline Hybrid Vehicle / Accurso, Francesco; Zanelli, Alessandro; Rolando, Luciano; Millo, Federico. - In: SAE TECHNICAL PAPER. - ISSN 0148-7191. - ELETTRONICO. - 1:(2020). [10.4271/2020-01-1009]

Availability:
This version is available at: 11583/2816334 since: 2020-05-20T11:56:24Z

Publisher:
SAE TECHNICAL PAPER

Published
DOI:10.4271/2020-01-1009

Terms of use:

This article is made available under terms and conditions as specified in the corresponding bibliographic description in the repository

Publisher copyright
GENERICO -- per es. Nature : semplice rinvio dal preprint/submitted, o postprint/AAM [ex default]

The original publication is available at https://saemobilus.sae.org/content/2020-01-1009/ / http://dx.doi.org/10.4271/2020-01-1009.

(Article begins on next page)

19 April 2024

2020-01-1009

Real Time Energy Management Control Strategies for an Electrically Supercharged Gasoline Hybrid Vehicle

Francesco Accurso, Alessandro Zanelli, Luciano Rolando, and Federico Millo

Politecnico di Torino

Abstract

The high level of electric power available on a Hybrid Electric Vehicle (HEV) enables the introduction of electrical auxiliaries in addition or in substitution to the ones currently available on a conventional powertrain. Among these auxiliaries, electric Superchargers (eSC) for the improvement of the vehicle performance or electrically heated catalysts for the reduction of the light-off time of the after-treatment may dramatically affect the Energy Management System (EMS) of an HEV. Moreover, since these devices are only fluid-dynamically, but not mechanically, linked to the powertrain, they are traditionally neglected in the optimization of the powersplit between internal combustion engine and electric machines by the EMS. The aim of the current work is the development of an EMS that is able to consider in real time the overall electric energy consumption of the entire powertrain. More in detail, this activity focuses on the refinement of the Equivalent Consumption Minimization Strategy (ECMS) including the power required by an eSC installed on a turbocharged gasoline engine. This innovative EMS is tested by means of numerical simulation on a small SUV (Sport Utility Vehicle) featuring a 48 V electric network over Type Approval and Real Driving Emissions (RDE) driving cycles. The novel EMS shows promising results in terms of eSC energy management and vehicle fuel consumption compared with the baseline.

Introduction

Powertrain electrification is nowadays commonly seen as the main solution for the reduction of CO_2 emissions in vehicles. This process progressively includes the substitution of traditional auxiliaries, as for example coolant pump, air conditioning compressor and air boosting devices with electrified ones. Concerning the electric boosting, an increasing interest has been observed in the last years. The electric boosting involves the integration of an electric machine between compressor and turbine in Electric Assisted Turbochargers (EAT) or the introduction in the engine airpath of an electrically driven compressor (or electric supercharger – eSC), typically in series with the main turbocharger. The advantage of EAT lies in the fact that the electric machine can be used to partially recover the engine exhaust energy [1-3]. This topic has been widely investigated in terms of thermodynamic potential on a passenger car Internal Combustion Engine (ICE) under steady operation by Vitek et al. [4] where little potential to improve the engine steady state performance of ICE was shown. On the other hand, electric superchargers are a promising electrified boosting solution [5] for the improvement of the torque response of downsized turbocharged engines thanks to a prompt activation (below 0.3 s).

In previous papers [6,7] the Authors investigated, by means of an integrated vehicle model, the impact of the eSC on performance and fuel consumption of Spark Ignition (SI) engines along type-approval and Real Driving Emissions (RDE) cycles. These works proved that improvements up to 15 % in term of vehicle performance could be achieved and fuel consumption reduction up to 9 % when the eSC was used as high efficiency concept enabler was observed. In [8] a similar study was performed on a λ=1 SI engine proving also in this case significant benefits on both performance and fuel economy,

Currently, several approaches could be exploited to integrate the electric boosting system in the engine control strategy. Heuristic control techniques were developed by Zanelli at al. [6, 7], by Griefnow et al. [9] for mild hybrid gasoline powertrains and by Schaub et al. [10] for mild hybrid diesel powertrain. Model Predictive Control (MPC) was also investigated by Liu [11] on a small Diesel engine with variable geometry turbine and exhaust gas recirculation valve. Nevertheless, these methodologies may lack of global perspective when integrated in a hybrid powertrain. As a matter of fact, the control of the electrified boosting system usually aims to maximize the power or the efficiency of the thermal machine while the EMS separately optimizes the powersplit between engine and electric motors. This is also true for high performance application, as presented by Ebbesen et al. [12] and by Salazar et al. [13, 14] where the control of a hybrid electric race car powertrain is developed for the reduction of the lap-time, but the electrically assisted turbocharger is only used as generator. Therefore, a comprehensive Energy Management System (EMS) dealing with both eSC and electric machines may lead to further improvements of both fuel economy and vehicle performance. In this context the Equivalent Consumption Minimization Strategy (ECMS) technique, firstly studied by Paganelli et al. [15] for the choice of the optimal powersplit, seems to represent a promising solution for the development of a controller able to comprehensively optimize the power flows of the entire powertrain including electric auxiliaries. As an example, an interesting application of the ECMS in an innovative powertrain featuring a motor which can be connected to a compressor (in electric supercharging mode) or directly to the crankshaft providing hybrid functionalities was proposed by Nazari et al. [16]. This hybrid powertrain was optimized for fuel consumption minimization by means of an offline ECMS, showing appealing results (more than 30 % reduction of fuel consumption).

The present paper presents a refinement of an online ECMS that includes eSC activation and operation, in a B-SUV vehicle model featuring a mild hybrid powertrain equipped with a λ=1 engine. This case study was already presented in a previous work [8]. The aim of the present work is to develop a real time control capable to predict the electric power needed for eSC activation and to optimize its operation for minimum CO_2 emissions. This control strategy has the objective to exploit the different power sources, the thermal engine and the Electric Machines (EMs), mechanically (the BSG) or not (the eSC) connected to the powertrain in order to achieve the highest powertrain efficiency. This innovative eSC controller was tested, and compared with respect to the Rule-Based controller developed in [6], on the type approval WLTC (Worldwide Harmonized Light-Duty Test Cycle) and on a more dynamic RDE driving cycle defined from the base of WLTC, defined as "standardized random test for an aggressive driving style" and known with the acronym RTS-95 [17].

Methodology

In this section a complete description of the case study is presented. Afterwards, a comprehensive overview of the methodology adopted for the numerical analysis is reported.

Case Study

The test case is a compact Sport Utility Vehicle (SUV) equipped with a 48 V electrified powertrain and a 6-speed manual transmission. The main vehicle specifications are given in Table 1.

Table 1. Main vehicle specifications for the Worldwide Harmonized Light-Duty Vehicles Test Cycle (WLTC) and the standardized random test for an aggressive driving style (RTS-95).

Vehicle Mass	1630 kg
Rolling Radius	333 mm
Power Demand @ 100 km/h (evaluated at wheel)	17.6 kW
Electric Load (engine on)	400 W
Electric Load (engine off)	120 W

The hybrid powertrain is a P0 architecture numerically assessed by the Authors in a previous work [9]. The propulsion system features a gasoline ICE coupled with a 48V liquid cooled Belt-Starter Generator (BSG). The electric machine is powered by a 48V Li-Ion Battery integrated in a dual voltage electric network (12 V + 48 V). In Table 2 and Table 3 the Li-Ion battery and BSG specifications are reported respectively.

Table 2. Specifications for the 48 V Li-Ion Battery

Nominal Voltage	48 V
Capacity	10 Ah
Min / Max Current	-250 / 250 A
Min / Max Voltage	32.5 / 54 V

Table 3. Specifications for the 48 V Belt Starter Generator (BSG)

Nominal Voltage	48 V
Peak Power (Generation, Braking)	18 kW
Continuous Power (Generation)	8 kW
Peak Power (Motoring)	12 kW

As far as the engine is concerned, a fully-stoichiometric gasoline turbocharged engine concept was numerically assessed [8], using the commercial software GT-SUITE. This stoichiometric engine concept was developed from a conventional EU5 gasoline engine whose main features are reported in Table 4.

Table 4. Engine Specifications

Displacement	1368 cm3
Compression Ratio	9.8
Rated Power	121 kW @ 5500 RPM
Rated Torque	250 Nm @ 2250 RPM
Fuel Metering System	Port Fuel Injection
Air Management System	VVA

The developed engine concept features the following modifications with respect to the base engine:

- λ=1 combustion among the overall engine map was adopted to guarantee the compliance with the future severe Conformity Factors (CFs) for NOx, PN, and CO evaluated during real driving operation, which may come in force with the oncoming Euro 6d emission regulations [18,19].
- Higher Temperature withstand turbine (increased from 930 °C to 980 °C). The adoption of a state of the art turbine, able to operate with very high exhaust gases temperature was considered an unavoidable technological improvement working with λ=1 combustion, while preserving the rated power of the engine, as presented in [20].
- A Knock Limited Spark Advance (KLSA) operation was exploited, taking advantage of a considerable margin from knock of the base engine. A refined knock model was adopted in order to recalibrate the spark-advance targeting an unburned gas fraction of 2% at knock onset. The increased spark-advance operation allowed both to reduce the exhaust gas temperatures in the high load region, and to obtain a considerable improvement of the engine efficiency.
- The base Compression Ratio (CR) of the engine was increased to 12.
- A Miller cycle has been adopted, aiming, in the low speed region, to decrease the knock likelihood enhanced with the higher CR and the KLSA operation; at higher engine speed, with the objective to decrease the exhaust gases temperature in order to get benefits in term of rated power.
- An electrically driven supercharger (eSC) was integrated in this configuration. The main specifications of the eSupercharger are shown in Table 5. While at high engine speed the TurboCharger (TC) is able to satisfy the boost pressure requirement of the Miller cycle, at low engine speed an electrically driven supercharger need to be introduced since the TC works at surge limit.

Table 5. eSupercharger main specifications

Compressor Max Speed	75000 RPM
Compressor Max Pressure Ratio	1.5
Compressor Max Corrected Mass Flow	0.10 kg/s
Compressor Peak Efficiency	0.82
Electric Motor Nominal Voltage	48 V
Electric Motor Max Torque	0.6 Nm
Electric Motor Max Power	5.3 kW

As highlighted by Millo et al. [8], the developed stoichiometric engine achieves a rated power similar to the base engine (4 kW lower) and features a LET (Low End Torque) performance considerably improved, thanks to the Miller cycle and to the eSupercharger.

Engine and Vehicle Model

An integrated vehicle model was developed by using the commercially-available software GT-SUITE. The model features a 1D computational fluid dynamics (CFD) Fast Running Model (FRM) engine, a 6-gear manual transmission and an electric network. The 1D-CFD FRM engine was developed and correlated with the experimental data of the reference engine in a previous work of the Authors [21]. The vehicle driver is simulated by means of a Proportional-Integral (PI) controller that defines the required power and the brake pedal based on the deviation of the vehicle speed from the target defined by the driving cycle. The vehicle speed error is kept within a moving window defined by tolerances on speed (±2 km/h) and on time (±1 s). Since the selected transmission is manual, the gear shift is imposed for the WLTC and the RTS-95 driving cycles. The gear shift pattern was computed by means of the Heinz Steven's tool made available by the UNECE committee [22], according to the UE Commission Regulation [23].

For the engine control, the engine speed and the target torque defined by the driver controller establish as setpoints a target level of boost pressure and intake manifold pressure. In a similar way, the intake valves lift profile is selected on the basis of the target torque and the engine speed. As far as the combustion is concerned, an imposed Wiebe profile has been adopted, that is function of the 50 % of the Mass Fraction Burned angle (MFB-50) and the experimentally measured 10% to 90% Mass Fraction Burned angular duration (MFB-10-90).

The target boost and intake manifold pressures and MFB-50 maps are beforehand computed in steady-state conditions, considering the typical limitations for a turbocharged gasoline engine: compressor surge, knock, maximum turbine inlet temperature (T3) and maximum turbocharger speed. As a matter of fact, the MFB-50 is defined in such a way that, starting from a value equal to 8 CA aTDC - assumed to be the optimum value corresponding to the Maximum Brake Torque (MBT) timing -, the combustion is retarded until the computed knock index falls below a safety threshold. On the other hand, the experimental MFB-10-90 of the reference engine was adopted for the analysis.

Hybrid Control Strategy

As far as the Hybrid Control Strategy is concerned, in this work a simple supervisory controller defines the optimum operating HEV mode considering all the system variables such as for example required power demand, engine speed, battery State of Charge (SoC), battery current and voltage limitations. More in detail, the supervisory controller defines one of the HEV functionalities listed here below:

- Stop-Start: the engine is switched off at a vehicle speed close to zero eliminating the fuel consumption during vehicle stops
- Regenerative Braking: partial recovery of the vehicle kinetic energy by the EM during deceleration phases. In line with the work done by Zanelli et al. [7], in this work the power request to the BSG follows a rule-based approach defined by the brake pedal request. As a matter of fact, the electric machine power request is null below a brake pedal request of 10% and grows linearly up to the full exploitation of the braking power of the BSG when the brake pedal request is equal to 60%.
- Parallel Mode: during traction phases the vehicle power demand is split between ICE and EM. This functionality can be subdivided in a Torque-Assist mode and in a Load Point Moving mode. On the one hand, the Torque-Assist decreases the power requested to the ICE, fulfilling the driver request by means of the further contribution of the EM. On the other hand, the Load Point Moving increases the ICE power demand with respect to the driver power demand recovering the surplus by means of the EM, used as a generator, and storing it into the battery.

When the powertrain operates in Parallel Mode, the EMS optimizes the powersplit between the ICE and the EM. In this study the Equivalent Consumption Minimization Strategy (ECMS) technique was adopted. The ECMS [15] defines the optimum powersplit at each time step by minimizing an instantaneous cost function. As described in [24], an equivalent fuel consumption can be associated with the use of electrical energy: under the hypothesis of charge sustaining condition, this fuel consumption is equivalent to the fuel flow required by the ICE to re-establish the battery SoC at the previous level. The battery equivalent fuel consumption can be summed to the actual fuel consumption to obtain the instantaneous equivalent fuel consumption $\dot{m}_{f,eq}$ as shown in Eq. 1:

$$\dot{m}_{f,eq} = \dot{m}_f + \dot{m}_{batt,eqv} = \dot{m}_f + \frac{s}{LHV} P_{batt} \qquad (1)$$

where $\dot{m}_f$ is the engine instantaneous fuel consumption (fuel mass flow rate), LHV is the fuel lower heating value, $\dot{m}_{batt,eqv}$ is the fuel consumption associated with the use of the electrical power, P_{batt} the power delivered or stored by battery. The term s is called equivalence factor and is used to convert electrical power into equivalent fuel consumption.

In order to keep the EMS control logic as simple as possible, steady state maps of the engine fuel consumption and of the electric to mechanic conversion efficiency of the BSG are used.

The hybrid control strategy was implemented using the commercially available software MATLAB-Simulink featuring an on-line powersplit optimization: for each time step the powersplit is defined as the combination of the P_{ICE} and P_{BSG} that minimizes the $\dot{m}_{f,eq}$. The requested engine brake torque and BSG brake torque are then exchanged with the physical model in the GT-SUITE environment.

As it is possible to highlight from Eq. 1, the ECMS considers only the electric power absorbed or delivered by the battery in the powersplit optimization. However, in an electric supercharged engine, the electric power required for the eSC activation is indirectly exploited for traction. As a matter of fact, it is converted into power to the fluid and consequently into mechanical power delivered by the engine, but it is not considered in the well-known ECMS optimization.

Control strategies for the real-time management of the concurrent control of BSG and eSC to manage the powersplit between these components in low voltage hybrid powertrains have already been presented in literature. For instance, in [25] a model based control technique has been developed, considering different costs of the electric energy (e.g. assuming free electric energy if coming from regenerative braking or assuming a fixed chemical to electrical conversion factor). Differently from [25], in the current study the electric power management was handled in a more comprehensive way, because it is integrated in the ECMS control strategy and the cost of the electric energy is defined on the basis of the charging opportunities over the driving cycle. This novel approach is indeed exploited for the fuel consumption minimization along different mission profiles by adopting an integrated ECMS in which the eSC utilization is considered as equivalent fuel flow rate.

For this purpose, the already presented Rule-Based controller for the eSC activation and operation developed by Zanelli et al. [6] was compared with a new control insight with the aim to integrate the electric power needed by the eSC in the ECMS energy management system.

eSC Rule-Based Controller

A Rule-Based controller was developed by the Authors [6] for the eSupercharger activation and regulation. The controller defines an operating condition for the eSC depending on the difference between the target boost pressure and the boost pressure reached by the main TC. The eSC is able to operate in a reduced engine map region (engine speed < 3000 RPM), due to the limited amount of mass flow rate that the device is able to operate with. If the engine speed is lower than the upper limit and there is a gap higher than a certain threshold in terms of actual and demanded boost, a target operating point in the eSC compressor map can be defined as the combination of a certain corrected mass flow rate and a pressure ratio. The latter is computed by sensing the pressure upstream and downstream the main turbocharger and taking into account the pressure losses of the low and high-pressure line (e.g. the intercooler pressure drop). The resulting eSC speed demand represents the control input for a PI controller which regulates the electric power supplied to the device. A bypass system, modelled as a controlled throttle valve, is introduced on the main airpath so that when the eSC is activated the system works as a series dual stage charging system, while when the eSC is deactivated it does not result in a flow restriction. Moreover, during deactivation the eSC is kept operating at idle speed of 5000 rpm to guarantee a prompt acceleration and to avoid too frequent high static load to the eSC bearings due to the start from zero speed. The eSC power request during the idle phases is about 20 W. The bypass valve opening and closure rate equal to ±450°/s is considered to take into account the physical actuation delay of the component. A graphical representation of the powertrain model including the eSC Rule-Based controller and the ECMS control logic is presented in Fig. A1 in the Appendix. Once the ECMS has chosen the optimal powersplit, the eSC is activated only if, from the engine torque request, a certain activation threshold is passed and a corresponding target speed is used to control the eSC. The electric power needed by the eSC is taken into account into the ECMS only as auxiliary power reducing the maximum available electric power from the battery. In this first control logic the eSC electric power is transparent to the ECMS for the choice of the optimal powersplit.

eSC controller integrated in ECMS

The base controller of the eSC was refined and integrated in the ECMS hybrid control strategy, featuring an integrated eSC-ECMS controller. The purpose is to account for the eSC activation and regulation energy consumption for each powersplit combination and use the ECMS energy management system as optimization technique for the choice and selection of the powersplit with minimum equivalent fuel consumption.

As it is possible to observe from Figure 1, during an activation, only a fraction of the electric power absorbed by the EM driving the eSC is transferred to the fluid and consequently contributing to the mechanical power provided by the ICE. In addition to the electromechanical power conversion losses, simulated by means of an efficiency map in GT-SUITE, a fraction of the supplied power is lost due to the friction of the device, modelled with a constant torque of 0.025 Nm applied to the eSC shaft. Moreover, considering the prompt activation of the eSC, during the first 0.2 s the mechanical power accelerates the eSC while the bypass valve opens. Hence, the mechanical power term can be split into three terms: friction power, inertia power and power transferred to fluid.

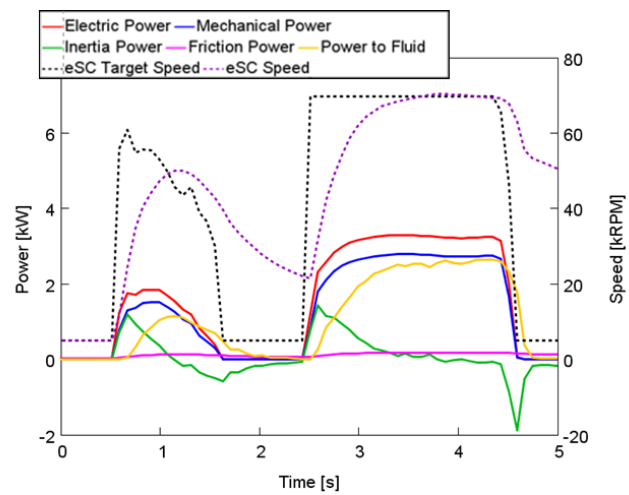

Figure 1. Analysis of power losses during during a transient eSC operation.

On the base of this preliminary analysis, the idea, that drives the development of a novel eSC control integrated in the EMS, is that for each powersplit combination it is possible to estimate the electric power required by the electric supercharger. The powersplit combination defined at each time-step by the ECMS (i.e. combination of ICE and EM driver power demand that satisfy the driver power demand) that minimizes the fuel consumption may include the inertia of system and all the losses terms encountered during the activation. To do so, firstly the eSC Rule-Based controller was integrated in the EMS as light supervisory layer for the eSC activation and a computation of the corresponding predicted eSC operating power is done. As a result, for each powersplit combination, a target eSC status (activation, regulation, deactivation) is defined, as well as a related electric power consumption that is included in the battery power considered by the ECMS. The eSC electric power request is computed at each time-step by the ECMS, as reported in Eq. 2:

$$P_{eSC} = (k \cdot P_{Steady} + P_{Inertia}) \cdot \frac{1}{\eta_{EM}} \quad (2)$$

P_{Steady} is the mechanical power required by the eSC considering a steady-state ICE power request. This term was beforehand computed by means of steady state engine simulation and a map was defined as function of RPM and Brake Torque. The $P_{Inertia}$ term, on the other hand, is computed instant by instant as reported in Equation 3.

$$P_{Inertia} = I \cdot \omega_{act} \cdot \frac{d\omega}{dt} \approx I \cdot \omega_{act} \cdot \frac{\omega_{tgt} - \omega_{act}}{t_{spool-up}} \quad (3)$$

I is the Moment of Inertia of the eSC, equal to 26.9 kg mm^2, ω is the eSC angular speed, the term $\frac{d\omega}{dt}$ is the angular acceleration. Assuming that the spool up time ($t_{spool-up}$) of the eSC is a constant for this component and equal to 0.25 s, the angular acceleration is proportional to the actual speed and the difference between target (ω_{tgt}) and actual angular speed (ω_{act}). The k coefficient in Eq. 2 is a correction factor that is used to correct the eSC steady state power requirement during transient operation. In this analysis, the gap between the actual state of the eSC and the target power was considered proportional to the ratio between the actual and target eSC speed. This latter corresponds to the steady state eSC speed. For this reason, k was computed as reported in Eq. 4.

$$k = \frac{\omega_{act}}{\omega_{tgt}} \quad (4)$$

The correction factor k is plotted in Figure 2 for the same eSC transient maneuver reported in Figure 1. As shown in Fig.2, the inertia of the system leads to a deviation of the eSC speed from the target speed. The correction factor k is adopted in Eq. 2 assuming that the steady state eSC power requirement can be scaled through the actual speed of the eSC.

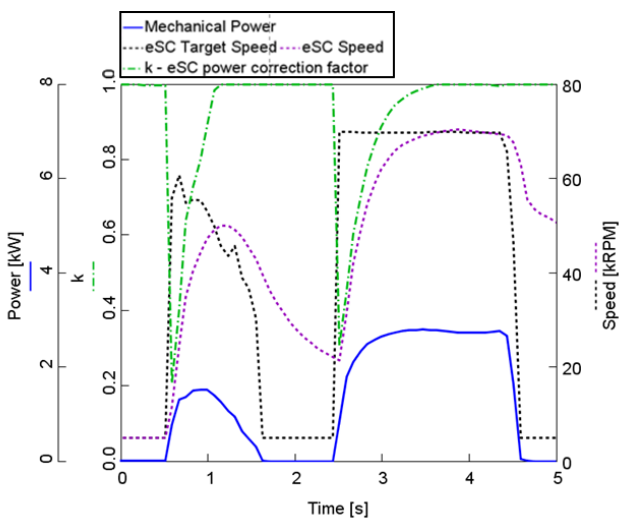

Figure 2. Highlight of the eSC power correction factor k during a transient eSC operation.

A complete overview of the refined ECMS control strategy that integrates the eSC power request in the consumption minimization for the optimal powersplit is depicted in Appendix, in Fig. A2.

The eSC activation may have a positive impact on engine efficiency (through pumping losses reduction), especially during maneuvers characterized by high power demands; this impact is not considered if using steady state maps for engine efficiency in the EMS control. However, the eSC allows the engine to achieve the target torque fast enough that the impact of this efficiency increase is quite limited along the driving cycle. More in details, the priority for the boost build-up is given to the WG and the eSC compensates uniquely the difference between target boost pressure and actual boost pressure. In this way, during a high power demand transient maneuver, the WG will close completely, thus limiting the transient benefit of the eSC on the pumping losses. Moreover, during a driving cycle, three different conditions may be observed. The first condition is for a low increase in the target torque, which corresponds to a low increase in the required boost pressure. In this case the threshold used in the control of the eSC prevents the eSC activation, and, as consequence, there is no impact at all on engine efficiency. Then, the second condition occurs when the target torque request increases reaching intermediate levels: in this condition the activation of the eSC has negligible impact on engine efficiency since the duration of this transient is typically quite limited and the WG is kept closed. Finally, the third condition occurs when the required boost pressure is high, with target torque values which correspond to engine operating map regions where the eSC needs to be activated even in steady state operation: in this condition, the impact of the eSC on engine efficiency is already included in the fuel consumption map of the engine. Finally, during the activation of the eSC the electric power is mainly used to accelerate the compressor, while the power transferred to the fluid is negligible (i.e. no impact on pumping losses and on engine efficiency). To sum up, the inaccuracies coming from the adoption of this simplified control approach appear to be more than acceptable.

Results

A comparison between the two eSC controllers is reported in this section. In order to have a consistent comparison, the proposed analysis was carried out with the same value of equivalence factor s for both the eSC controllers, equal to 2 for the WLTC and 1.92 for the RTS-95. These values were calibrated for the WLTC and for the RTS-95 separately, in order to achieve a difference of the depleted or added battery energy below 0.2 % of the fuel energy over the driving cycle. In this way it is possible to focus on the impact of the eSC controller on the results. Firstly, the capability to predict the eSC power is assessed. Afterwards, the eSC energy consumption along the driving cycle and the impact on the overall fuel consumption are presented. Furthermore, a sensitivity analysis on the eSC activation threshold and on the impact of the added or depleted energy in the battery at the end of the driving cycle is carried out.

eSC Controller

Starting the analysis from the eSC control capability to predict the eSC power request, a comparison between simulation results and ECMS prediction is given in Figure 3 and Figure 4 for the WLTC and RTS-95 respectively. As it is possible to figure out from the bottom chart of the these two figures, the ECMS is able to accurately estimate the inertia power contribution during the eSC activation. The mechanical power prediction can be considered satisfactory. The slight deviation is due to the map-based approach used for the estimation of the eSC power in steady-state condition. This approach assumes that friction power, mass flows and pressure ratio during the activation transient linearly increase with the eSC speed rise. As a matter of fact, this approach slightly overestimates the electric power request during the

early stages of the activation while underestimates this power request slightly before the eSC deactivation. This latter behavior may be explained by the fact that a PI controller ultimately controls the eSC. This controller reacts to the change in boost request with a delay and it is for this reason anticipated by the estimation of the power directly from a map. For these reasons, this simple prediction model can be used directly in the ECMS energy management logic.

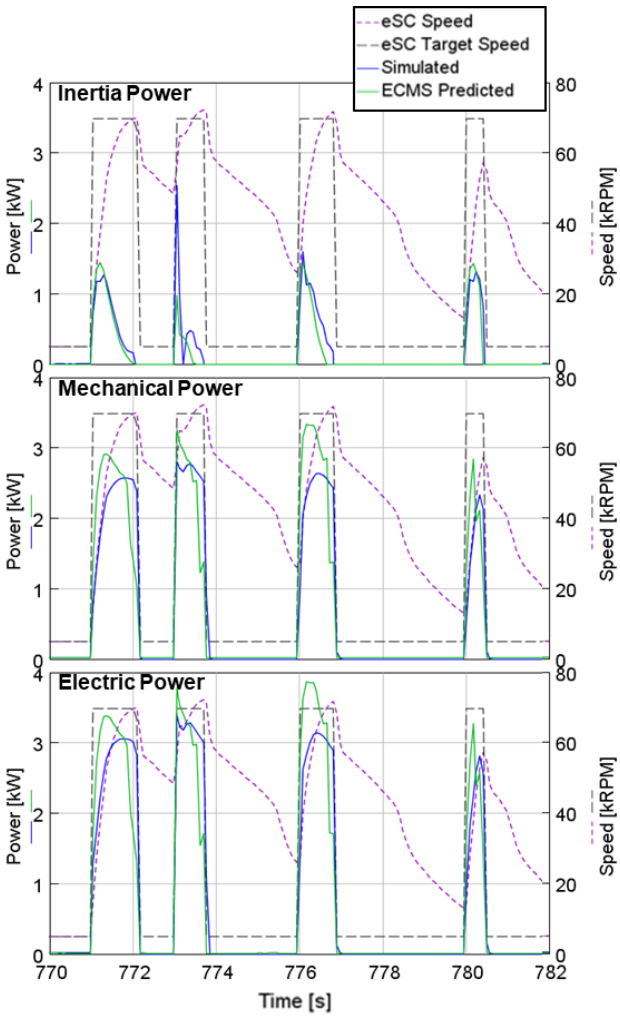

Figure 3. Analysis of the eSupercharger (eSC) controller on a portion of the WLTC: eSC target speed in grey dashed line, eSC speed in violet dashed line, eSC simulated power in blue solid line and eSC power predicted by the ECMS in green solid line.

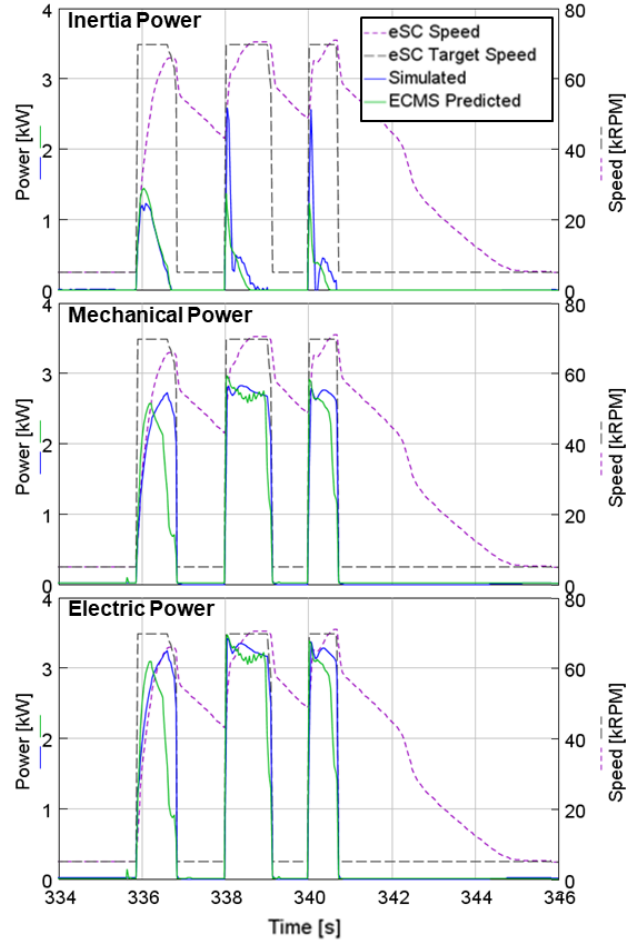

Figure 4. Analysis of the eSupercharger (eSC) controller on the RTS-95: eSC target speed in grey dashed line, eSC speed in violet dashed line, eSC simulated power in blue solid line and eSC power predicted by the ECMS in green solid line.

Moving to the comparison between the Rule-Based and the ECMS-integrated eSC control, a remarkable difference in terms of utilization of the supercharger can be pointed out from Figure 5. The cumulated energy consumption along the driving cycles, referred as eSC electric energy in the top charts of the two figures, considerably reduces if the eSC power is considered by the ECMS. In addition, from the bottom chart of the figures it is possible to quantify the useful energy fraction provided by the eSC to the fluid. Considering the electromechanical losses in the EM and the energy lost during the idle operations, the amount of energy transferred to the fluid across the compressor is about the 50% of the electric energy provided to the eSC electric motor. The ratio between the energy transferred to the fluid and the electric energy, referred as supercharging efficiency, is reported in the bottom chart of the Fig. 5. The ECMS-integrated controller reduces the utilization of the eSC along the driving cycle. This reduction leads to an increase of the idle operation and consequently to a lower level of the supercharging efficiency, that reduces from 0.52 with the Rule-Based controller to 0.47 with the updated eSC controller, due to the increase of the impact of the power required for idle operation.

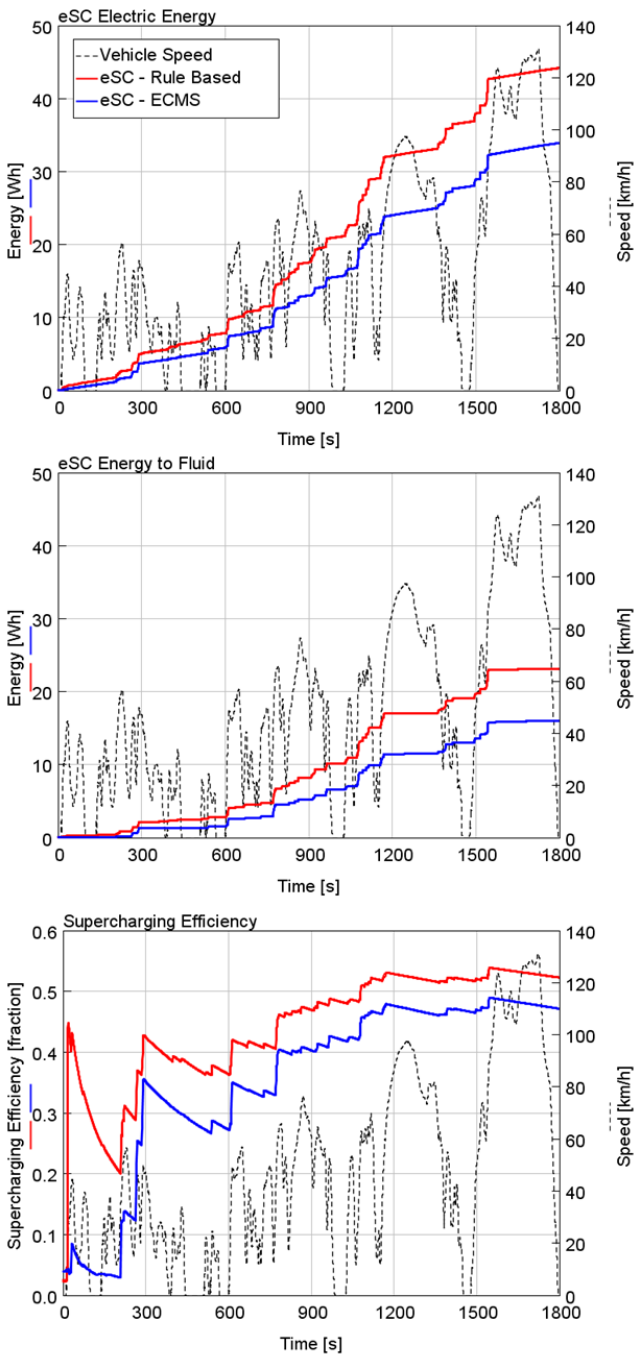

Figure 5. Cumulated eSupercharger (eSC) energy consumption in the upper chart, cumulated energy transferred to the fluid in the middle chart and supercharging efficiency in the bottom chart along the WLTC: vehicle speed in grey dashed line, eSC energy with Rule-Based controller in red solid line and eSC energy with ECMS-integrated controller blue solid line.

The values of electric energy and energy transferred to the fluid for both the WLTC and the RTS-95 are plotted in Figure 6.

The eSC energy consumption is reduced by 10.2 Wh (more than 20%) with the refined ECMS-integrated eSC controller on the WLTC and by 4.2 Wh (about 9%) on the RTS-95. The difference between the two driving cycles is due to the higher driver power demand on the RTS-95 with respect to the WLTC, which constrains the ICE to operate at high load and consequently to widely exploit the eSupercharger.

Consequently, the electrically supercharging operation is charaterized by a higher efficiency on the RTS-95 with respect to the WLTC (supercharging efficiency equal to 0.63 for both the Rule-Based and the ECMS-Integrated eSC controller).

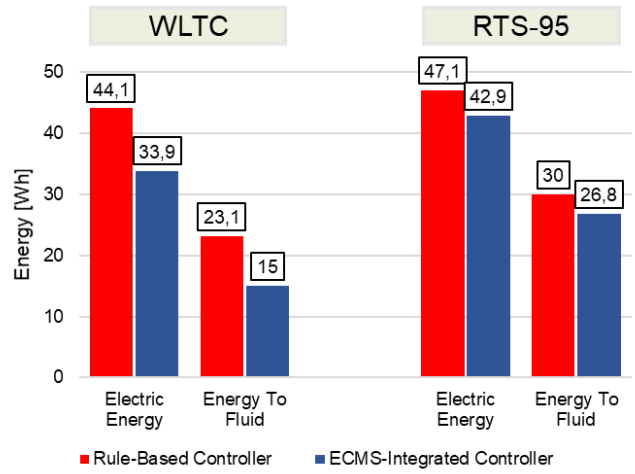

Figure 6. Total eSC energy consumption and energy transferred to the fluid on the WLTC and RTS-95 driving cycles: Rule-Based controller in red, ECMS.integrated controller in blue.

Sensitivity Analysis to the Activation Criteria

In order to gather a deeper understanding of the main differences in terms of eSC operation between the base and the refined controller a sensitivity analysis to the eSC activation criteria was carried out. More in detail, the eSC is activated if the difference between the target and the actual boost pressure is larger than a defined threshold. For the reference case, stated as Case A for the subsequent analysis, the boost pressure threshold is equal 0.4 bar. This value was reduced to 0.1 with the aim to investigate the impact of a different threshold for the eSC activation (Case B).

Table 6. eSupercharger main specifications

	Case A	Case B
Boost Pressure Difference for Activation	0.4 bar	0.1 bar

As shown in Figure 7 for the WLTC and in Figure 8 for the RTS-95, the reduction of the pressure difference threshold leads, as expected, to an increase of the eSupercharger operation along the two driving cycles.

Focusing on the Rule-Based controller, comparing Case A to Case B, the eSC energy consumption increases by 13.5 Wh (+23%) on the WLTC and by 15.6 Wh (+25%) on the RTS-95. A similar trend can be outlined also with the refined eSC-integrated controller. In this case the energy is increased by 8.5 Wh (+20%) on the WLTC and by 10.3 Wh (+19%) on the RTS-95. The increase in energy required by eSC is due to the fact that, by lowering the activation threshold, the electric supercharger is more frequently activated. Also for Case B, the ECMS-integrated controller leads to a lower energy consumption of the eSC if compared to the Rule-Based controller, consistently with Case A.

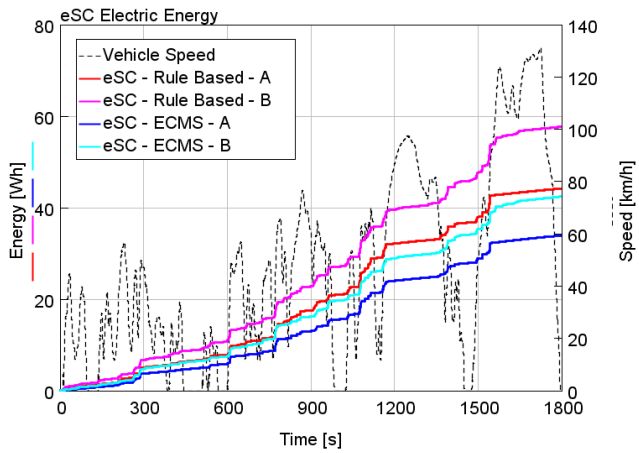

Figure 7. Cumulated eSupercharger (eSC) energy consumption along the WLTC: eSC speed in grey dashed line, eSC simulated power in blue solid line and eSC power predicted by the ECMS in green solid line.

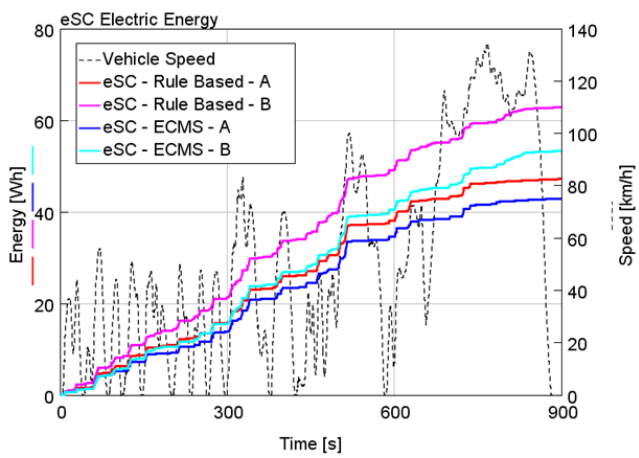

Figure 8. Cumulated eSupercharger (eSC) energy consumption along the WLTC: eSC speed in grey dashed line, eSC simulated power in blue solid line and eSC power predicted by the ECMS in green solid line.

Fuel Consumption Evaluation

Moving to the fuel consumption evaluation, the values of CO_2 emissions are reported in Figure 9 and Figure 10, evaluated on the WLTC and on the RTS-95 respectively. The CO_2 emissions were evaluated in charge sustaining condition, namely a neutral energy balance of the stored battery energy at the start and at the end of the driving cycle. To do so, the formula of the integral formulation of the ECMS was used to compute the CO_2 emissions corresponding to the stored or depleted battery energy. The expression is reported in Eq 5:

$$\frac{gCO_{2,batt}}{km} = \frac{s}{LHV}\,\Delta E_{batt}\,\xi\,\frac{1}{distance} \tag{5}$$

Where ΔE_{batt} is the added or depleted battery energy and ξ is the fuel to CO_2 conversion factor (i.e. the grams of CO_2 produced per gram of fuel burned, equal to 3.167 for a fuel with an H/C ratio of 1.85). The hypothesis behind this formulation is that if the term ΔE_{batt} is close to zero, the equivalence factor s is representative of the chemical to electric energy conversion. For this reason, it can be used also to convert the amount of energy depleted or added in the battery in an equivalent CO_2 emission in g/km. In this analysis, for all the cases presented in the previous section, the absolute value of ΔE_{batt} is lower than 0.2 % of the fuel energy over the cycle, and the equivalence factor s (2 for the WLTC and 1.92 for the RTS-95) was used to compute the battery equivalent CO_2 emissions. The charge-sustaining CO_2 emissions results are computed as reported in Eq 6:

$$\frac{gCO_{2,corr}}{km} = \frac{gCO_2}{km} + \frac{gCO_{2,batt}}{km} \tag{6}$$

As it is possible to point out from Fig. 9, the CO_2 emissions increases if the eSC activation threshold is lowered to 0.1 bar with the Rule-Based controller. The higher energy requirement for the eSC operation results in a CO_2 penalty. Considering on the other hand the ECMS-integrated controller, there is not a clear advantage with the base eSC activation threshold of 0.4 bar with respect to the reference controller. On the other hand, it effectively reduces the CO_2 emissions penalty for the Case B, keeping the fuel consumption at a similar level of the Case A, equal to 158.8 gCO_2/km. The CO_2 emissions reduction with the refined controller is 0.4 gCO_2/km on the WLTC.

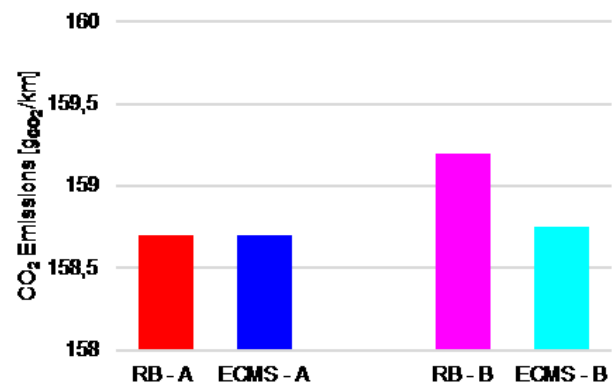

Figure 9. CO_2 emissions evaluated on the WLTC in charge sustaining condition.

Similar results can be outlined also if the fuel consumption is evaluated according to the RTS-95 driving cycle, as can be shown in Figure 10. In this case the CO_2 emissions are at similar level with the base eSC controller for Case A and Case B. With the refined ECMS the CO_2 emissions reduced up to 0.4 gCO_2/km in Case B.

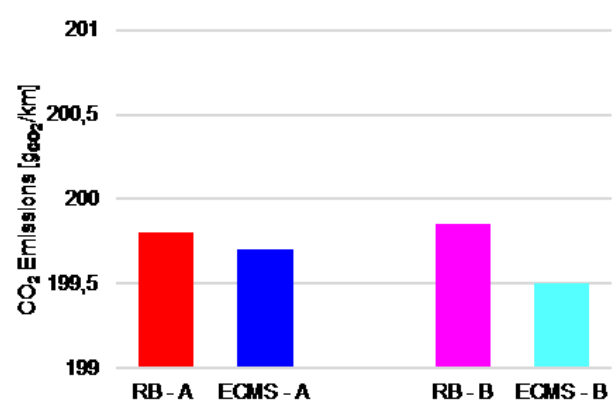

Figure 10. CO_2 emissions evaluated on the RTS-95 in charge sustaining condition.

From this result it is possible to conclude that the ECMS-integrated eSC turns out to be effective in terms of fuel consumption reduction if the amount of energy handled by the electrically driven supercharger becomes larger. This was confirmed also with the subsequent sensitivity analysis on the End-of-Cycle battery energy.

Sensitivity Analysis to the End-of-Cycle battery energy

This further sensitivity analysis is focused on the impact that the end-of-cycle depleted or added battery energy has on the two-eSC controller performance. A depleted or added energy at the end of the cycle translates in the possible increase or decrease of the electric power that can be provided to the auxiliaries by the battery to guarantee charge sustaining at the end of the cycle. This sensitivity analysis has been done on the RTS-95 driving cycle to ideally investigate the impact of electric auxiliaries power on a RDE test. For this analysis the equivalence factor has been varied in the range between 1.7 to 2.3. The result of this analysis is represented in Fig. 10, where the higher boost threshold level is considered (Case A) for the two eSC controllers. Likewise, Case B scenario (lower threshold for eSC activation) is shown in Fig. 11 for the two eSC controllers. Fig. 11 and Fig. 12 show the impact on BSG energy consumption for traction purpose (i.e. only when the BSG is used as a motor), eSC energy consumption and CO_2 emissions with respect to the depleted or added energy in the battery. The orange area on the left indicates that the electric auxiliary energy virtually reduces to zero for those cases which show a depleted battery equal or below to -75 Wh. In the top picture of Fig. 11, the BSG energy consumption is shown and this quantity reduces linearly as the energy in the battery increases showing how the ECMS control strategy reduces the amount of provided traction power of the BSG to keep more energy in the battery that is ultimately recovered by regenerative braking. Indeed, for this case study the load point moving used to recharge the battery is seldom applied by the EMS. In the middle picture the eSC energy consumption is shown. The eSC requires a constant amount of energy (lower when the eSC controller is integrated in the ECMS) up to an added battery energy of 50 Wh. For higher amount of stored energy, the eSC energy consumption increases linearly due to the fact that the reduced torque assist from the BSG pushes the engine to operate at higher load where the eSC has to be activated and operated. Finally, in the lower picture the CO_2 emissions are shown. The CO_2 emissions increase as the battery charge increases at the end of the cycle. Across the entire analysis, when Case A is considered, there is little difference between the impact that the two different controllers have on the fuel consumption.

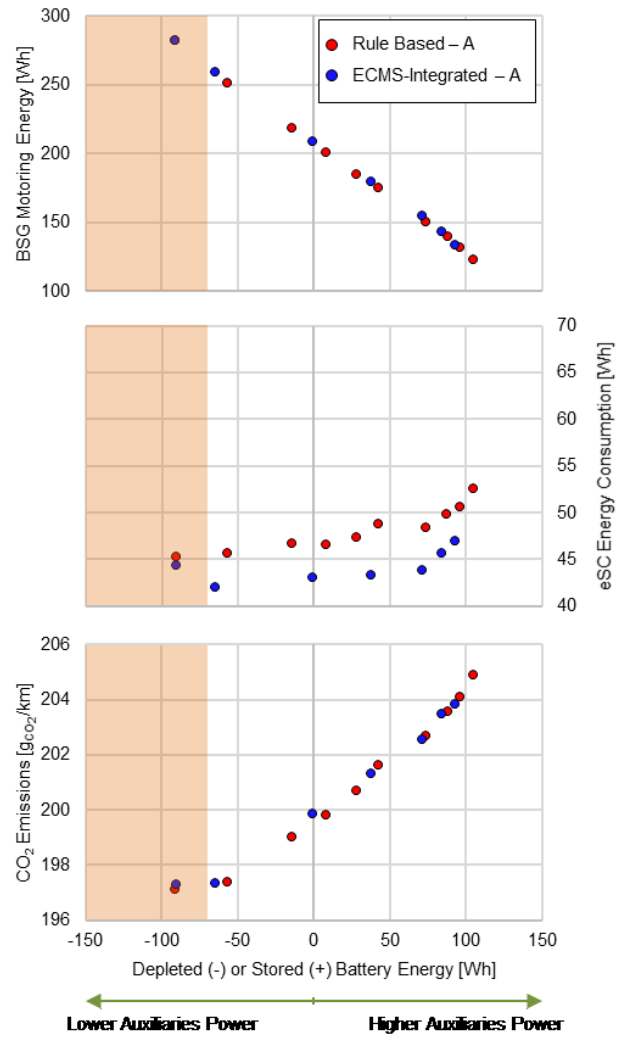

Figure 11. Sensitivity analysis to the depleted or stored energy in the battery on the RTS-95 driving cycle. Case A.

On the other hand, if the case B is considered, it is possible to highlight a slight improvement in terms of fuel economy. Looking at the bottom chart of Fig. 12, the CO_2 emissions are reduced with the ECMS-integrated eSC controller for the entire sweep of End-of-Cycle battery energy. At large values of stored energy (around 100 Wh equivalent to an increase of the auxiliary power of 400 W on the RTS-95) a significant CO_2 emission reduction can be highlighted from the chart (about 0.6 gCO_2/km at 100 Wh stored battery energy). As already mentioned, the refined eSC controller becomes effective in terms of CO_2 emission reduction if the eSC operation and the related energy consumption increase.

The refined hybrid control strategy shows a greater fuel consumption saving potential if the electric energy absorption by the auxiliaries becomes larger, and, because of the imposed charge sustaining condition, the cost of the electric power for the propulsion is larger as well. In these conditions, the CO_2 benefits that can be achieved with the presented integrated EMS is larger than 0.5 g/km in comparison with the Rule-Based approach. Moreover, considering the current trend in ICE based powertrain electrification and the extensive introduction in the vehicle of electrical auxiliaries (e.g. electrically driven air conditioning compressor or water pump, electrically heated

catalyst etc.) the energy absorption by the auxiliaries is expected to further increase and the proposed integrated EMS could therefore lead to even more significant CO_2 emissions reductions.

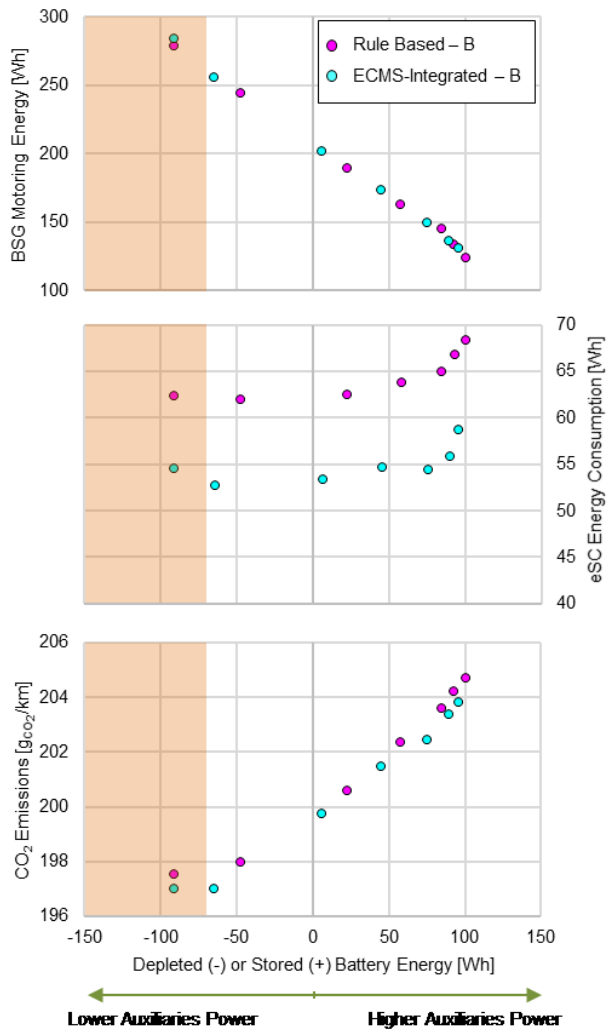

Figure 12. Sensitivity Analysis to the depleted or stored energy in the battery on the RTS-95 driving cycle. Case B.

Conclusions

This paper proposed an innovative controller for an electrified boosting system, in particular for an electric supercharger in series with the main turbocharger in a downsized turbocharged gasoline engine. The innovative controller, which integrates the eSC activation and electric power request in the EMS of the mild hybrid vehicle and adopts the ECMS logic, reduced the eSC energy requirement by 20% in the WLTC and by 9% in the RTS-95. Although this reduction produced only a little impact on the fuel consumption (up to 0.4 gCO_2/km on the RTS-95), the innovative controller provides the benefit of a reduced sensitivity to the calibration parameters of the conventional Rule-Based control. The novel hybrid control strategy showed a greater fuel economy benefits if the electric energy stored in the battery increases (more than 0.5 gCO_2/km of CO_2 reduction with a 100 Wh stored battery energy on the RTS-95). This enables a more efficient utilization of the electric energy on RDE cycles, where the power required by the electric auxiliaries is typically higher with respect to type-approval driving cycles. Within such a perspective, the fuel consumption reduction potential of the developed EMS may be further enhanced in a vehicle featuring different electric boosting devices or extensively adopting vehicle electric auxiliaries (e.g. electrically driven air conditioning compressor, water pump, electrically heated catalyst etc.).

This analysis therefore provides a contribution to the development of vehicle energy management strategy with the aim to take into account the entire electric power flow of electric boosting devices, which are usually neglected in the optimization of the powersplit.

References

1. Millo, F., Mallamo, F., Pautasso, E., and Ganio Mego, G., "The Potential of Electric Exhaust Gas Turbocharging for HD Diesel Engines," SAE Technical Paper 2006-01-0437, 2006, https://doi.org/10.4271/2006-01-0437.
2. Wei, W., Zhuge, W., Zhang, Y., & He, Y. (2010, October). Comparative study on electric turbo-compounding systems for gasoline engine exhaust energy recovery. In *ASME Turbo Expo 2010: Power for Land, Sea, and Air* (pp. 531-539). American Society of Mechanical Engineers.
3. Zhuge, W., Huang, L., Wei, W., Zhang, Y. et al., "Optimization of an Electric Turbo Compounding System for Gasoline Engine Exhaust Energy Recovery," SAE Technical Paper 2011-01-0377, 2011, https://doi.org/10.4271/2011-01-0377.
4. Vitek, O. and Macek, J., "Thermodynamic Potential of Electrical Turbocharging for the Case of Small Passenger Car ICE under Steady Operation," SAE Technical Paper 2017-01-0526, 2017, https://doi.org/10.4271/2017-01-0526.
5. Spinner, G., Dahinten, F., Dauscher, S., & Münz, S. (2018, April). Electrified boosting systems in today's and future automotive applications. In 2018 Thirteenth International Conference on Ecological Vehicles and Renewable Energies (EVER) (pp. 1-5). IEEE.
6. Zanelli, A., Millo, F., Barbolini, M., and Neri, L., "Assessment through Numerical Simulation of the Impact of a 48 V Electric Supercharger on Performance and CO2 Emissions of a Gasoline Passenger Car," SAE Technical Paper 2019-01-1284, 2019, https://doi.org/10.4271/2019-01-1284.
7. Zanelli, A., Millo, F., and Barbolini, M., "Driving Cycle and Elasticity Manoeuvres Simulation of a Small SUV Featuring an Electrically Boosted 1.0 L Gasoline Engine," SAE Technical Paper 2019-24-0070, 2019, https://doi:10.4271/2019-24-0070.
8. Millo, F., Accurso, F., Zanelli, A., Rolando, L. "Numerical Investigation of 48 V Electrification Potential in Terms of Fuel Economy and Vehicle Performance for a Lambda-1 Gasoline Passenger Car," *Energies* **2019**, *12*, 2998.
9. Griefnow, P., Andert, J., Xia, F., Klein, S. et al., "Real-Time Modeling of a 48V P0 Mild Hybrid Vehicle with Electric Compressorfor Model Predictive Control," SAE Technical Paper 2019-01-0350, 2019, https://doi:10.4271/2019-01-0350.
10. Schaub J., Frenken C., Holderbaum B., Griefnow P., Savelsberg R., Coppin O. (2017) FEV ECObrid – a 48V mild hybrid concept for passenger car Diesel engines. In: Liebl J., Beidl C. (eds) Internationaler Motorenkongress 2017. Proceedings. Springer Vieweg, Wiesbaden. doi: /10.1007/978-3-658-17109-4_15
11. Liu, Y., Wang, Y. Y., Canova, M. (2018, June). Distributed Model Predictive Control of an Electrically Boosted Diesel Engine Air Path System. In *2018 Annual American Control Conference (ACC)* (pp. 2461-2466). IEEE.

12. Ebbesen, S., Salazar, M., Elbert, P., Bussi, C., Onder, C. H. (2017). Time-optimal control strategies for a hybrid electric race car. *IEEE Transactions on Control Systems Technology*, *26*(1), 233-247.
13. Salazar, M., Elbert, P., Ebbesen, S., Bussi, C., Onder, C. H. (2017). Time-optimal control policy for a hybrid electric race car. *IEEE Transactions on Control Systems Technology*, *25*(6), 1921-1934.
14. Salazar, M., Balerna, C., Elbert, P., Grando, F. P., Onder, C. H. (2017). Real-time control algorithms for a hybrid electric race car using a two-level model predictive control scheme. *IEEE Transactions on Vehicular Technology*, *66*(12), 10911-10922.
15. Paganelli, G.; Guerra, T.M.; Delprat, S.; Santin, J.J.; Delhom, M.; Combes, E. Simulation and assessment of power control strategies for a parallel hybrid car. Proc. Inst. Mech. Eng. Part D J. Automobil. Eng. 2000, 214, 705–717.
16. Nazari, S., Middleton, R., Siegel, J., and Stefanopoulou, A., "Equivalent Consumption Minimization Strategy for a Power Split Supercharger," SAE Technical Paper 2019-01-1207, 2019, doi:10.4271/2019-01-1207.
17. https://www.dieselnet.com/standards/cycles/index.php accessed Nov. 16, 2019.
18. Clairotte, M., Valverde, V., Bonnel, P., Giechaskiel, B., Carriero, M., Otura, M., Fontaras, G., Pavlovic, J., Martini, G., Krasenbrink, A. "Joint Research Centre 2017 Light-Duty Vehicles Emissions Testing," Publications Office of the European Union: Luxembourg, 2018; ISBN 978-92-79-90601-5.
19. Scharf, J., Thewes, M., Balazs, A., Fh, D., Lückenbach, S., Speckens, F., "All Clean Gasoline Hybrid Powertrains—Real Driving Emissions, Lambda = 1 & Euro 7," In Proceedings of the Aachen Colloquium Automobile and Engine Technology, Aachen, Germany, 8–10 October 2018; pp. 935–956.
20. Glahn, C., Koenigstein, D.A., Hermann, I. "Future for All?—Lambda-1-Combustion Systems of Small Powertrains for the High Volume Market," In Proceedings of the Aachen Colloquium Automobile and Engine Technology, Aachen, Germany, 8–10 October 2018; pp. 913–934.
21. Millo, F., Di Lorenzo, G., Servetto, E., Capra, A. et al., "Analysis of the Performance of a Turbocharged S.I. Engine under Transient Operating Conditions by Means of Fast Running Models," *SAE Int. J. Engines* 6(2):968-978, 2013, https://doi.org/10.4271/2013-01-1115.
22. https://wiki.unece.org/display/trans/Gearshift+calculation+tool, accessed Nov. 16, 2019.
23. COMMISSION REGULATION (EU) 2017/1151, OJ L 175, 7.7.2017, pp. 1–643. Available online: https://eur-lex.europa.eu/legal-content/EN/TXT/?uri=OJ:L:2017:175:TOC, accessed Nov. 16, 2019.
24. Onori, S., Serrao, L., & Rizzoni, G. (2016). *Hybrid electric vehicles: energy management strategies* (Vol. 13). Berlin Heidelberg: Springer.
25. Griefnow, P., Andert, J., Birmes, G., Pischinger, S., "Optimierungsbasiertes Energiemanagement für 48-V-Mildhybrid-Antriebe," ATZ Extra 24, 42–47 (2019) doi:10.1007/s35778-019-0015-5

Contact Information

Federico Millo
Energy Dept., Politecnico di Torino
C.so Duca degli Abruzzi, 24
10129, Turin, ITALY
Phone: +39 011 0904517
federico.millo@polito.it

Acknowledgments

The valuable support provided to this research activity by FCA is gratefully acknowledged. In particular, the Authors would like to thank Caterina Venezia, Davide Peci, Giovanni Guenna and Constantinos Vafidis for their precious and constant support as well as for their invaluable suggestions during the simulation activities.

Definitions/Abbreviations

aTDC	After Top Dead Center
BSG	Belt Starter Generator
CF	Conformity Factor
CFD	Computational Fluid Dynamics
CR	Compression Ratio
EAT	Electrically Assisted Turbocharger
ECMS	Equivalent Consumption Minimization Strategy
ECU	Engine Control Unit
EM	Electric Machine
EMS	Energy Management System
eSC	eSupercharger
FRM	Fast Running Model
HEV	Hybrid Electric Vehicle
ICE	Internal Combustion Engine
KLSA	Knock-Limited Spark Advance
MBT	Maximum Brake Torque
MFB-10-90	10–90% Mass Fraction Burned Angular Duration
MFB-50	50% Mass Fraction Burned Angle
MPC	Model Predictive Control
PI	Proportional Integral
RDE	Real Driving Emissions

RTS-95	Standardized Random Test For An Aggressive Driving Style
SI	Spark Ignition
SoC	State of Charge
SUV	Sport Utility Vehicle
T3	Turbine Inlet Temperature
TC	Turbocharger
VVA	Variable Valve Actuation
WG	Wastegate
WLTC	Worldwide Harmonized Light-Duty Test Cycle

List of Symbols

$\frac{gCO_2}{km}$	Specific CO_2 emissions
$\frac{gCO_{2,batt}}{km}$	Specific equivalent CO_2 emissions computed from the depleted or stored battery energy
$\frac{gCO_{2,corr}}{km}$	Specific corrected CO_2 emissions
I	eSC moment of inertia
k	eSC power correction factor
LHV	Fuel lower heating value
$\dot{m}_{batt,eqv}$	Fuel flow rate associated with the battery power
$\dot{m}_f$	ICE fuel flow rate
$\dot{m}_{f,eq}$	Equivalent fuel flow rate
P_{batt}	Battery power
P_{BSG}	BSG mechanical power
P_{eSC}	eSC electric power
P_{ICE}	ICE mechanical power
P_{Steady}	eSC steady-state mechanical power
s	Equivalence factor
$t_{spool-up}$	Acceleration time of the eSC from idle speed to maximum speed
ΔE_{batt}	Stored or depleted battery energy
η_{EM}	eSC electric motor efficiency
λ	Relative Air-to-Fuel Ratio
ξ	Fuel to CO_2 conversion factor
ω	eSC angular speed
ω_{act}	eSC actual angular speed
ω_{tgt}	eSC target angular speed

Appendix

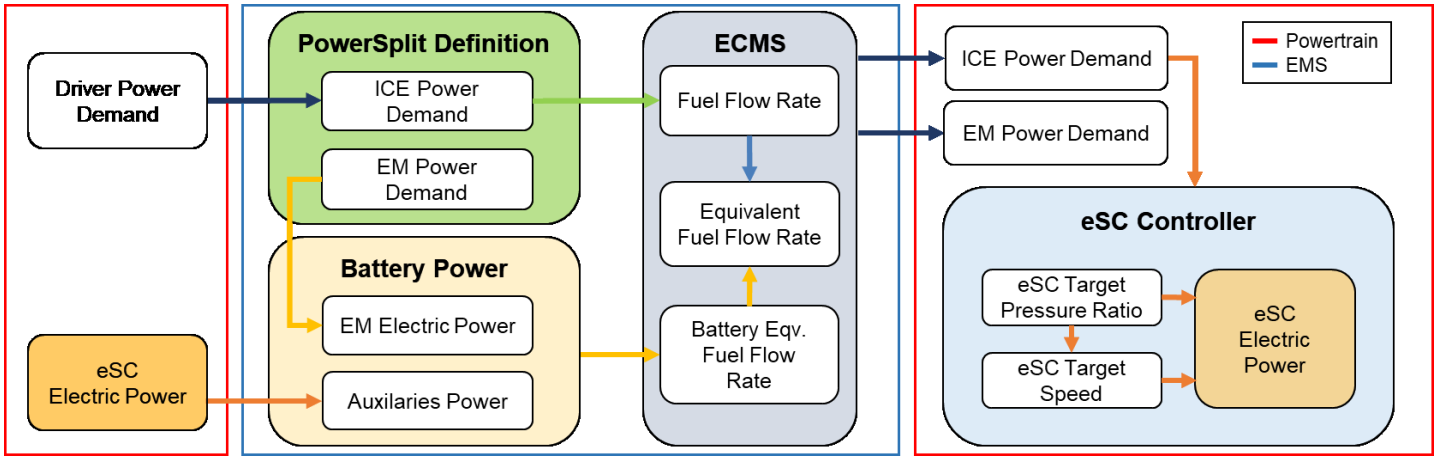

Figure A1. Schematic representation of the powertrain model including the eSC Rule-Based controller and the ECMS control logic.

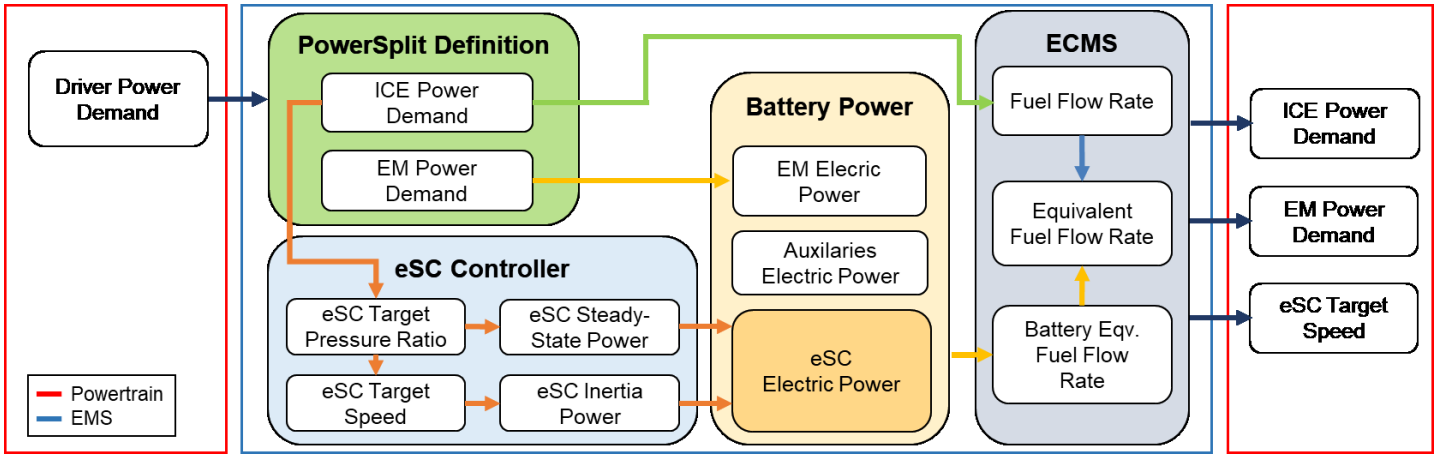

Figure A2. Schematic representation of the powertrain model including the ECMS control logic, which integrates the eSC controller.